Cell Tissue Res, DOI 10.1007/s00441-016-2415-9

Identification of a shootin1 isoform expressed in peripheral tissues

Yasuna Higashiguchi[1], Kazuhiro Katsuta[1], Takunori Minegishi[1], Shigenobu Yonemura[2], Akihiro Urasaki[1], Naoyuki Inagaki[1]

[1]Laboratory of Systems Neurobiology and Medicine, Graduate School of Biological Sciences, Nara Institute of Science and Technology, Ikoma, Nara 630-0192, Japan.

[2]Department of Cell Biology, Institute of Biomedical Sciences, Tokushima University Graduate School, Kuramoto-cho, Tokushima 770-8504, Japan

Email: Naoyuki Inagaki, ninagaki@bs.naist.jp

Abstract

Shootin1 is a brain-specific cytoplasmic protein involved in neuronal polarity formation and axon outgrowth. It accumulates at the leading edge of axonal growth cones, where it mediates the mechanical coupling between F-actin retrograde flow and cell adhesions, as a clutch molecule, thereby producing force for axon outgrowth. In this study, we report a novel splicing isoform of shootin1 which is expressed not only in the brain but also in peripheral tissues. We renamed the brain-specific shootin1 as shootin1a and termed the novel isoform as shootin1b. Immunoblot and immunohistochemical analyses with a shootin1b-specific antibody revealed that shootin1b is distributed in various mouse tissues including the lung, liver, stomach, intestines, spleen, pancreas, kidney and skin. Interestingly, shootin1b immunoreactivity was detected widely in epithelial cells that constitute simple and stratified epithelia; in some cells, it colocalized with E-cadherin and cortactin at cell-cell contact sites. Shootin1b also localized in dendritic cells in the spleen. These results suggest that shootin1b may function in various peripheral tissues including epithelial cells.

Keywords: Shootin1b, Clutch molecule, Epithelial cell, Dendritic cell

Introduction

The linkage between the actin cytoskeleton and cell adhesions plays essential roles in cell-cell interaction, cellular morphogenesis and migration (Suter and Forscher, 2000; Le Clainche and Carlier, 2008; Yonemura, 2011; Brieher and Yap, 2013). In motile cells, actin filaments polymerize at the leading edge and disassemble proximally (Pollard and Borisy, 2003; Le Clainche and Carlier, 2008), which, in conjunction with myosin II activity, induces retrograde flow of actin filaments (Wang, 1985; Forscher and Smith, 1988; Katoh, et al., 1999; Mallavarapu and Mitchison, 1999). Mechanical coupling between actin filament flow and cell adhesions by "clutch" molecules is thought to play key roles in producing force for axon outgrowth and cell migration (Mitchison and Kirschner; 1988, Suter and Forscher, 2000; Thievessen, et al., 2013; Toriyama, et al., 2013; Garcia, et al., 2015).

Shootin1 is a recently identified brain-specific clutch molecule (Toriyama, et al., 2006; Shimada, et al., 2008) that is involved in axon outgrowth and neuronal polarity formation (Toriyama, et al., 2010; Inagaki, et al., 2011; Sapir, et al., 2013). In cultured hippocampal neurons, shootin1 couples mechanically the actin filament retrograde flow and the cell adhesions at the leading edge of axonal growth cones, through the actin-binding protein cortactin (Weed and Parsons, 2001; MacGrath and Koleske, 2012) and the cell adhesion molecule L1-CAM (Kamiguchi, et al., 1998), and produces force for axon outgrowth (Kubo, et al., 2015). This coupling is positively regulated by the chemoattractant netrin-1 through PAK1-mediated shootin1 phosphorylation (Toriyama, et al., 2013; Kubo, et al., 2015). A recent report also demonstrates that shootin1-mediated cytoskeletal-adhesion coupling contributes to an intracellular transport of actin and actin-associated proteins along axons (Katsuno, et al., 2015).

In this study, we report a novel splicing isoform of shootin1, shootin1b, which is expressed not only in the brain but also in peripheral tissues. To provide insights into the functions of shootin1b, we examined its tissue localization using an antibody which specifically recognizes shootin1b. Our data show that shootin1b is expressed in various cells including epithelial cells and dendritic cells in peripheral tissues.

Materials and Methods

All relevant aspects of the experimental procedures were approved by the Institutional Animal Care and Use Committee of Nara Institute of Science and Technology.

Cloning of shootin1b

Full-length cDNA encoding rat shootin1b was amplified by PCR from a rat brain cDNA library (Clontech Laboratories) with the primers 5'-CCGCTCGAGATGAACAGCTCGGACGAGGAGAAG and 5'-CCGCTCGAGTCAGCAGTTAGAACTGTCCGTCTC. To produce a shootin1b-specific antibody, cDNA encoding the C-terminal region (amino acid residues 454-633) of rat shootin1b was amplified by PCR with the primers 5'-CGGGATCCGGGACACTTAACAAACCCAC and 5'-CCGCTCGAGTCAGCAGTTAGAACTGTCCGTCTC. The cDNAs were then subcloned into the pGEX vector (GE Healthcare).

Protein and antibody preparation

Protein and antibody preparation were performed as described (Toriyama, et al., 2006). In brief, recombinant full-length and C-terminal regions of shootin1b were expressed in *Escherichia coli* as GST fusion proteins and purified on a glutathione-Sepharose column (GE Healthcare), after which GST was removed by PreScission protease (GE Healthcare). A rabbit polyclonal anti-shootin1b antibody was raised against the recombinant C-terminal region of shootin1b and affinity-purified before use.

Immunoblot

Immunoblotting was performed as described previously (Inagaki, et al., 1997). Adult (2-5 months) and embryonic day (E) 18.5 mouse tissues were diced into small pieces in RIPA lysis buffer (50 mM Tris-HCl, pH 8.0, 1 mM EDTA, 150 mM NaCl, 1% Triton X-100, 0.1% SDS, 0.1% sodium deoxycholate, 2 mM phenylmethylsulfonyl fluoride, 5 μg/ml leupeptin, 10 mM NaF and 1mM DTT) and sonicated. After a 15-min incubation on ice, protein extracts were centrifuged at 17,500g for 15 min at 4°C. After mixing with SDS loading buffer and incubating at 95°C for 5 min, the protein extracts and purified proteins were electrophoresed on 8% polyacrylamide gels and transferred to PVDF membranes. After blocking with blocking buffer (0.05% Tween-20, 3% non-fat dried milk in Tris-buffered saline) for 1 h at room temperature, the membranes were incubated with anti-shootin1 antibody (1:200 dilution in blocking buffer), anti-shootin1b antibody (1:20,000) or anti-actin antibody (1:5,000) overnight at 4°C. After washing, membranes were incubated with horseradish peroxidase (HRP)-linked anti-rabbit antibody (1:2,000) or HRP-linked anti-mouse antibody (1:5,000) for 1 h at room temperature. Immunoreactive bands were

visualized by the ECL Western Blotting Detection system (GE Healthcare).

Cell culture

EpH4 cells from mouse mammary glands (Reichmann, et al., 1989) (provided by Dr. E. Reichman, University Children's Hospital, Zurich, Switzerland) were cultured at 37°C in a humid atmosphere of 5% CO_2 and 95% air in Dulbecco's modified Eagle's medium (Sigma) supplemented with 10% FBS (Invitrogen).

Immunohistochemistry, immunocytochemistry and microscopy

Immunohistochemistry and immunocytochemistry were performed as described (Inagaki, et al., 1988; Inagaki, et al., 1997), with slight modifications. Briefly, mouse tissues were dissected and trimmed to allow efficient penetration of the fixative. After fixation by 4% paraformaldehyde (PFA), tissues were dehydrated with 30% sucrose and embedded in Tissue-Tek O.C.T. Compound (Sakura) and cut into 8-μm sections on a Cryostat. The sections were washed and blocked with blocking buffer (10% normal goat serum or 10% Fetal bovine serum in phosphate buffer with 0.3% Triton X-100) for 2 h at room temperature. Samples were incubated with anti-shootin1b (1:20,000 dilution in blocking buffer), anti-TFF2 (1:200), anti-Mist1 (1:200), anti-cytokeratin-19 (1:50), anti-albumin (1:200), anti-amylase (1:200), anti-E-cadherin (1:1,000), anti-cortactin (1:100) or anti-CD11c (1:100) overnight at 4°C, and then incubated with Alexa Fluor 488-conjugated anti-Rabbit IgG (H+L) (1:1,000), Alexa Fluor 594-conjugated anti-Mouse IgG (H+L) (1:1,000) or Alexa Fluor 594-conjugated anti-Armenian hamster IgG (H+L) (1:500) overnight at 4°C. After washing, cell nuclei were stained with 4,6-diamidino-2-phenylindole (DAPI). For preparation of the data in Fig. S3, two serial sections of skin and forestomach were immunostained: one section stained with anti-shootin1b antibody and the other stained without the antibody. Their photographs were taken at the same exposure time.

EpH4 cells were fixed with 1% formaldehyde in phosphate buffered saline (PBS) for 15 min at room temperature. After washing with PBS, the cells were treated with 0.2% Triton X-100 in PBS for 10 min at room temperature and blocked with blocking buffer (10% fetal bovine serum in PBS) for 1 h at room temperature. They were then incubated with anti-shootin1b (1:10,000 dilution in blocking buffer) together with anti-E-cadherin (1:200) or anti-cortactin (1:100) overnight at 4°C, and incubated with Alexa Fluor 488-conjugated anti-Rabbit IgG (H+L) (1:1,000) and Alexa Fluor 594-conjugated anti-Mouse IgG (H+L) (1:1,000) for 1 h at room temperature.

Fluorescence images were acquired using a confocal microscope (LSM 700 or LSM 710; Carl Zeiss) equipped with a EC Plan-Neofluar 10x 0.30 M27, a plan-Apochromat 20x 0.8 M27, a plan-Apochromat 40x 1.3 oil DIC M27 and a plan-Apochromat 63x 1.40 oil M27

objectives (Carl Zeiss) and imaging software (ZEN2009; Carl Zeiss). The acquired images were processed using Adobe Photoshop.

RT-PCR

Total RNA was extracted from the cornified layer and whole skin of P5 mouse by using TRIzol (Thermo Fisher Scientific) according to manufacturer's instructions, and then treated with RQ1 RNase-free DNase (Promega). Fifty ng of total RNA was used for cDNA synthesis using M-MLV Reverse Transcriptase (Promega) and Random Primer (Takara). PCR was performed with the cDNA as a template and ExTaq HS (Takara). Primers used for RT-PCR are as follows: 5'-ATAGCAGTAGTCCTACCGGGATATT-3' (shootin1b forward), 5'-TTTTCTCCTGTATCCACCTTTACTG-3' (shootin1b reverse), 5'-TGTTACCAACTGGGACGACA-3' (β-actin forward), and 5'-GGGGTGTTGAAGGTCTCAAA-3' (β-actin reverse).

Materials

C57BL/6 mice were obtained from SLC Japan and CLEA Japan. Preparations of shootin1a and the antibody against shootin1 were described elsewhere (Toriyama, et al., 2006). DAPI was obtained from Roche Diagnostics. Monoclonal antibodies against CD11c (N418, Armenian hamster), TFF2 (GE16C, mouse) and Mist1 (6E8/A12/C11P1, mouse) were obtained from Abcam. Monoclonal antibodies against amylase (G-10, mouse), cortactin (4F11, mouse) and E-cadherin (mouse) were obtained from Santa Cruz Biotech, Millipore and BD Transduction Laboratories, respectively. Polyclonal antibodies against cytokeratin-19 (N-13, goat) and albumin (goat) were obtained from Santa Cruz Biotech and Bethyl laboratories, respectively. HRP-linked anti-rabbit IgG, Alexa Fluor 488-conjugated anti-Rabbit IgG (H+L), Alexa Fluor 594-conjugated anti-Rabbit IgG (H+L), Alexa Fluor 594-conjugated anti-Mouse IgG (H+L), Alexa Fluor 594-conjugated anti-Armenian hamster IgG (H+L), Alexa Fluor 488-conjugated anti-goat IgG (H+L) and Alexa Fluor 488-conjugated anti-mouse IgM were obtained from GE Healthcare, Thermo Fisher Scientific, Jackson ImmunoResearch, Life Technologies, Jackson ImmunoResearch, Invitrogen and Invitrogen, respectively. Anti-actin antibody (C4, mouse) and HRP-linked anti-mouse IgG were obtained from Millipore and BioRad, respectively.

Results

Identification of shootin1b and preparation of its specific antibody

Immunoblot analyses of E18.5 mouse brain lysate with anti-shootin1 antibody revealed an immunoreactive band at 87 kD, in addition to the 60-kD band corresponding to shootin1 (Toriyama, et al., 2006) (Fig. 1a). Database searches identified mouse, rat and human splice variants of shootin1 which encodes proteins of 631, 633 and 631 amino acids, respectively, with a predicted molecular mass of 71.3 kD, 71.4 kD and 71.3 kD, respectively (accession no.: mouse, NP_001107784.1; rat, ABK56023.1; human, NP_001120683.1) (Fig. 1b and Fig. S1a). We renamed the original shootin1 as shootin1a (accession no.: mouse, ABK56021.1; rat, ABK56023.1; human, ABK56022.1) and refer to the novel isoform as shootin1b. In mouse shootin1b, the three amino acids ASQ at the C-terminus of shootin1a (residues 454-456) are substituted by 178 amino acid residues (Fig. 1c-c' and Fig. S1b). In addition, similar proteins have been predicted in other organisms such as *Macaca mulatta* (accession no.: XP_002805879.1), *Canis lupus* (accession no.: XP_005637827.1), *Bos taurus* (accession no.: XP_003587946.2), *Gallus gallus* (accession no.: XP_421781.3) and *Xenopus (Silurana) tropicalis* (accession no.: XP_004915785.1).

We then cloned the cDNA for rat shootin1b, and raised an antibody against the shootin1b-specific region (amino acid residues 454-633) of rat shootin1b. Immunoblot analyses with this antibody recognized rat recombinant shootin1b at 87 kD and an 87-kD band in E18.5 mouse brain lysate (Fig. 1a'), thereby demonstrating the expression of shootin1b in the embryonic brain. This antibody did not detect the 60-kD band corresponding to shootin1a in the immunoblot of mouse brain lysate, indicating that it recognizes specifically shootin1b. Similar data were obtained using E18.5 rat brain lysates (data not shown).

Shootin1b is widely distributed in adult and developmental tissues

Next, we examined the expression of shootin1b in the mouse brain and peripheral tissues using immunoblot analysis. Shootin1b was highly expressed in the embryonic brain but could not be detected in the adult brain (Figs. 1d-d' and S2). In contrast to the brain-specific shootin1a (Toriyama, et al., 2006), shootin1b was detected widely in adult peripheral tissues including the lung, liver, stomach, small intestine, large intestine, spleen, pancreas, kidney and skin, and in embryonic peripheral tissues including the lung, stomach, small intestine, large intestine, pancreas, kidney and skin (Figs. 1d-d' and S2).

Localization of shootin1b in the skin

We next examined the localization of shootin1b in adult and E18.5 peripheral tissues by immunohistochemical analyses using the shootin1b-specific antibody; shootin1b localization in

the brain will be reported separately. In adult and embryonic mouse skin, intense shootin1b immunoreactivity was detected in all layers of the epidermis (the basal/germinal, spinous and granular layers), which constitute a stratified squamous epithelium (Fig. 2a-a''' and 2b-b'''), and in the hair follicles (Fig. 2b'''). On the other hand, shootin1b-immunoreactive cells were sparse in the dermis (Fig. 2a-a' and 2b-b'), and the sebaceous gland lacked shootin1b immunoreactivity (Fig. 2a' and 2a'''). The cornified layer showed very strong immunofluorescence; however, we do not rule out the possibility that this involves nonspecific immunostaining, because the cornified layer showed immunofluorescence even in the absence of the anti-shootin1b antibody (Fig. S3a and b). So, we analyzed the expression of shootin1b mRNA by RT-PCR. The shootin1b PCR product was detected both in the cornified layer and whole skin of P5 mice (Fig. S4), suggesting that shootin1b is expressed in the cornified layer. Interestingly, shootin1b accumulated at the cell-cell contact sites of some epithelial cells in the epidermis and hair follicles (arrowheads, Fig. 2a''' and 2b''-b''').

Localization of shootin1b in the gastrointestinal tract

Figs. 3-5 show shootin1b immunoreactivity in the gastrointestinal tract. The murine stomach consists of two functionally distinct compartments: the forestomach, which has a keratinized squamous epithelium, and the glandular stomach with a simple columnar epithelium (Troy, et al., 2007). In the adult and E18.5 forestomach, unkeratinized cells of the stratified squamous epithelium were intensely stained by the anti-shootin1b antibody (Fig. 3a-a'' and 3b-b''). Although the keratinized layer also showed immunofluorescence, we do not rule out the possibility that this represents nonspecific immunostaining because of immunofluorescence in the absence of the anti-shootin1b antibody (Fig. S3c and d). The simple columnar epithelium of the adult and E18.5 glandular stomach showed immunoreactivity for shootin1b (Fig. 4a-a''' and b-b''). We performed double staining of the adult glandular stomach with the antibodies against a neck cell marker secretory protein TFF2 (Syu et al., 2012) and a chief cell marker transcription factor Mist1 (Ramsey et al., 2007). As shown in Fig. 4c-c'''', the neck zone which contains TFF2 positive mucous neck cells, showed relatively weak shootin1b-immunoreactivity. On the other hand, shootin1b was expressed in Mist1-positive chief cells in the base zone (arrows, Fig. 4d''). The murine intestines also contain simple columnar epithelium. As shown in Fig. 5, the epithelia of the E18.5 small intestine and the adult and E18.5 large intestine were immunoreactive for shootin1b. In some of the epithelial cells in the stomach and intestines, shootin1b accumulated at the lateral membrane (arrowheads, Figs. 3-5).

Localization of shootin1b in other tissues

In the adult and E18.5 lung, the epithelia of the bronchus, which form a pseudostratified

epithelium, showed strong shootin1b immunoreactivity (Fig. 6a-a'' and b-b''). In addition, we observed shootin1b-immunoreactive non-epithelial cells scattered in the lung (arrows, Fig. 6b''). In the adult liver, strong shootin1b immunoreactivity was detected in the epithelial cells of the bile duct (Fig. 6c-c'') which are immunoreactive for a bile duct cell marker cytokeratin-19 (Wen et al., 2011) (arrowheads, Fig. 6d''). We also detected relatively weak immunoreactivity in cell-cell contact sites of the hepatic cells (arrows, Fig. 6c'') which are immunoreactive for a hepatic cell marker albumin (Yadav et al., 2009) (arrowheads, Fig. 6e''). In the adult and E18.5 pancreas (Fig. 7), the epithelial cells of the secretory duct as well as acinar cells, which are immunoreactive for an acinar cell marker amylase (Preis et al., 2011) (arrowheads, Fig. 7c''), were stained by the anti-shootin1b antibody. In some epithelial cells in the bile duct and the secretory duct of the pancreas, shootin1b accumulated at cell-cell contact sites (arrowheads, Figs. 6c'' and 7a'').

In the adult spleen, we observed shootin1b-immunoreactive non-epithelial cells (Fig. 8). The shootin1b-immunoreactive cells also showed immunoreactivity for CD11c, a marker for dendritic cells (Metlay, et al., 1990; Leenen, et al., 1998; McIlroy, et al., 2001) (arrows), suggesting that the dendritic cells in the spleen express shootin1b.

Shootin1b colocalizes with E-cadherin and cortactin at cell-cell contact sites

As described above, we noted that shootin1b accumulates at cell-cell contact sites of some of the epithelial cells examined here. Recently, we reported that cortactin interacts with shootin1a at axonal growth cones (Kubo, et al., 2015); shootin1b also contains the region responsible for the interaction with cortactin (amino acid residues 261-377 of shootin1a). In addition, cortactin accumulates at cadherin-based cell-cell contacts and is thought to regulate cell adhesions (El Sayegh, et al., 2004; Helwani, et al., 2004; Ren, et al., 2009; Truffi, et al., 2014). Finally, therefore, we analyzed the colocalization of shootin1b with E-cadherin and cortactin in epithelial cells in tissues and cultured cells. As shown in Fig. 9, shootin1b colocalized with E-cadherin and cortactin at cell-cell contact sites of epithelial cells of the epidermis and glandular stomach (arrowheads). In addition, shootin1b colocalized with E-cadherin and cortactin at cell-cell contact sites of cultured EpH4 epithelial cells, which are derived from mouse mammary glands (Fig. 10, arrowheads).

Discussion

Previous studies reported that shootin1a (formerly shootin1) mediates key processes in neuronal cells, including neuronal symmetry-breaking (Toriyama, et al., 2010; Inagaki, et al., 2011), polarity formation (Toriyama, et al., 2006; Sapir, et al., 2013), signal-mediated axon outgrowth (Toriyama, et al., 2013; Kubo, et al., 2015) and axonal transport (Katsuno, et al., 2015). Mechanically, shootin1a acts as a clutch molecule to couple actin filaments and cell adhesions, thereby generating the force underlying these processes (Shimada, et al., 2008; Katsuno, et al., 2015; Kubo, et al., 2015). In this study, we identified shootin1b, a novel splicing isoform of shootin1a. Shootin1b contains almost the entire amino acid sequence of shootin1a, including the three coiled-coil domains and a proline-rich region, and an additional C-terminal 178-residue region that is specific to shootin1b (Fig. 1c'). In contrast to shootin1a, which is detected only in the brain (Toriyama, et al., 2006), shootin1b was distributed not only in the brain but also in the lung, liver, stomach, small intestine, large intestine, spleen, pancreas, kidney and skin (Fig. 1d-d'). These data expand our view of shootin1-mediated cellular processes.

The present study showed that shootin1b accumulates at cell-cell contact sites of some epithelial cells, where it colocalizes with E-cadherin and the actin-binding protein cortactin. Recently, we found that cortactin interacts with shootin1a, as another clutch molecule, and mediates shootin1a-dependent axon outgrowth. Shootin1b also contains the region responsible for the interaction with cortactin (amino acid residues 261-377 of shootin1a) (Kubo, et al., 2015). Cortactin accumulates at cadherin-based cell-cell contacts and is thought to regulate cell adhesions (El Sayegh, et al., 2004; Helwani, et al., 2004; Ren, Helwani, et al., 2009; Truffi, Dubreuil, et al., 2014). The possible involvement of shootin1b in cell adhesions remains an important issue for future studies.

Shootin1b was also detected in non-epithelial cells including dendritic cells. As clutch molecules are thought to produce forces not only for axon outgrowth but also for cell migration (Suter and Forscher, 2000; Thievessen, et al., 2013; Craig, et al., 2015; Kubo, et al., 2015), shootin1b may play a role in the migration of non-neuronal cells. The mRNAs encoding shootin1a and shootin1b are derived from the same premature RNA (Fig. S1a). The mechanism regulating the differential production of mRNAs for shootin1b and shootin1a in different cell types is an intriguing problem that would merit further investigations.

Acknowledgements

EpH4 cells were the kind gift of Dr. E. Reichman. We thank Drs. Sadao Shiosaka and Michinori Toriyama for reviewing the manuscript.

Funding

This research was supported in part by JSPS Grant-in-Aid for Scientific Research on Innovative Areas (25102010), JSPS KAKENHI (26290007), Osaka Medical Research Foundation for Incurable Diseases and Mitsubishi Foundation.

References

Brieher WM, Yap AS (2013) Cadherin junctions and their cytoskeleton(s). Curr Opin Cell Biol 25:39-46

Craig EM, Stricker J, Gardel M, Mogilner A (2015) Model for adhesion clutch explains biphasic relationship between actin flow and traction at the cell leading edge. Phys Biol 12:035002

El Sayegh TY, Arora PD, Laschinger CA, Lee W, Morrison C, Overall CM, Kapus A, McCulloch CA (2004) Cortactin associates with N-cadherin adhesions and mediates intercellular adhesion strengthening in fibroblasts. J Cell Sci 117:5117-5131

Forscher P, Smith SJ (1988) Actions of cytochalasins on the organization of actin filaments and microtubules in a neuronal growth cone. J Cell Biol 107:1505-1516

Garcia M, Leduc C, Lagardere M, Argento A, Sibarita JB, Thoumine O (2015) Two-tiered coupling between flowing actin and immobilized N-cadherin/catenin complexes in neuronal growth cones. Proc Natl Acad Sci U S A 112:6997-7002

Helwani FM, Kovacs EM, Paterson AD, Verma S, Ali RG, Fanning AS, Weed SA, Yap AS (2004) Cortactin is necessary for E-cadherin-mediated contact formation and actin reorganization. J Cell Biol 164:899-910

Inagaki N, Goto H, Ogawara M, Nishi Y, Ando S, Inagaki M (1997) Spatial patterns of Ca2+ signals define intracellular distribution of a signaling by Ca2+/Calmodulin-dependent protein kinase II. J Biol Chem 272:25195-25199

Inagaki N, Toriyama M, Sakumura Y (2011) Systems biology of symmetry breaking during neuronal polarity formation. Dev Neurobiol 71:584-593

Inagaki N, Yamatodani A, Ando-Yamamoto M, Tohyama M, Watanabe T, Wada H (1988) Organization of histaminergic fibers in the rat brain. J Comp Neurol 273:283-300

Kamiguchi H, Hlavin ML, Yamasaki M, Lemmon V (1998) Adhesion molecules and inherited diseases of the human nervous system. Annu Rev Neurosci 21:97-125

Katoh K, Hammar K, Smith PJ, Oldenbourg R (1999) Birefringence imaging directly reveals architectural dynamics of filamentous actin in living growth cones. Mol Biol Cell 10:197-210

Katsuno H, Toriyama M, Hosokawa Y, Mizuno K, Ikeda K, Sakumura Y, Inagaki N (2015) Actin migration driven by directional assembly and disassembly of membrane-anchored actin filaments. Cell Rep 12:648-660

Kubo Y, Baba K, Toriyama M, Minegishi T, Sugiura T, Kozawa S, Ikeda K, Inagaki N (2015) Shootin1-cortactin interaction mediates signal-force transduction for axon outgrowth. J Cell Biol 210:663-676

Le Clainche C, Carlier MF (2008) Regulation of actin assembly associated with protrusion and adhesion in cell migration. Physiol Rev 88:489-513

Leenen PJ, Radosevic K, Voerman JS, Salomon B, van Rooijen N, Klatzmann D, van Ewijk W (1998) Heterogeneity of mouse spleen dendritic cells: in vivo phagocytic activity, expression of macrophage markers, and subpopulation turnover. J Immunol 160:2166-2173

MacGrath SM, Koleske AJ (2012) Cortactin in cell migration and cancer at a glance. J Cell Sci 125:1621-1626

Mallavarapu A, Mitchison T (1999) Regulated actin cytoskeleton assembly at filopodium tips controls their extension and retraction. J Cell Biol 146:1097-1106

McIlroy D, Troadec C, Grassi F, Samri A, Barrou B, Autran B, Debre P, Feuillard J, Hosmalin A (2001) Investigation of human spleen dendritic cell phenotype and distribution reveals evidence of in vivo activation in a subset of organ donors. Blood 97:3470-3477

Metlay JP, Witmer-Pack MD, Agger R, Crowley MT, Lawless D, Steinman RM (1990) The distinct leukocyte integrins of mouse spleen dendritic cells as identified with new hamster monoclonal antibodies. J Exp Med 171:1753-1771

Mitchison T, Kirschner M (1988) Cytoskeletal dynamics and nerve growth. Neuron 1:761-772

Pollard TD, Borisy GG (2003) Cellular motility driven by assembly and disassembly of actin filaments. Cell 112:453-465

Preis M, Gardner TB, Gordon SR, Pipas JM, Mackenzie TA, Klein EE, Longnecker DC, Gutmann EJ, Sempere LF, Korc M (2011) MicroRNA-10b expression correlates with response to neoadjuvant therapy and survival in pancreatic ductal adenocarcinoma. Clin Cancer Res 17:5812-5821

Ramsey VG, Doherty JM, Chen CC, Stappenbeck TS, Konieczny SF, Mills JC (2007) The maturation of mucus-secreting gastric epithelial progenitors into digestive-enzyme secreting zymogenic cells requires Mist1. Development 134:211-222

Reichmann E, Ball R, Groner B, Friis RR (1989) New mammary epithelial and fibroblastic cell clones in coculture form structures competent to differentiate functionally. J Cell Biol 108:1127-1138

Ren G, Helwani FM, Verma S, McLachlan RW, Weed SA, Yap AS (2009) Cortactin is a functional target of E-cadherin-activated Src family kinases in MCF7 epithelial monolayers. J Biol Chem 284:18913-18922

Sapir T, Levy T, Sakakibara A, Rabinkov A, Miyata T, Reiner O (2013) Shootin1 acts in concert with KIF20B to promote polarization of migrating neurons. J Neurosci 33:11932-11948

Shimada T, Toriyama M, Uemura K, Kamiguchi H, Sugiura T, Watanabe N, Inagaki N (2008) Shootin1 interacts with actin retrograde flow and L1-CAM to promote axon outgrowth. J Cell Biol 181:817-829

Suter DM, Forscher P (2000) Substrate-cytoskeletal coupling as a mechanism for the regulation

of growth cone motility and guidance. J Neurobiol 44:97-113

Syu LJ, El-Zaatari M, Eaton KA, Liu Z, Tetarbe M, Keeley TM, Pero J, Ferris J, Wilbert D, Kaatz A, Zheng X, Qiao X, Grachtchouk M, Gumucio DL, Merchant JL, Samuelson LC, Dlugosz AA (2012) Transgenic expression of interferon-γ in mouse stomach leads to inflammation, metaplasia, and dysplasia. Am J Pathol 181:2114-2125

Thievessen I, Thompson PM, Berlemont S, Plevock KM, Plotnikov SV, Zemljic-Harpf A, Ross RS, Davidson MW, Danuser G, Campbell SL, Waterman CM (2013) Vinculin-actin interaction couples actin retrograde flow to focal adhesions, but is dispensable for focal adhesion growth. J Cell Biol 202:163-177

Toriyama M, Kozawa S, Sakumura Y, Inagaki N (2013) Conversion of a signal into forces for axon outgrowth through Pak1-mediated shootin1 phosphorylation. Curr Biol 23:529-534

Toriyama M, Sakumura Y, Shimada T, Ishii S, Inagaki N (2010) A diffusion-based neurite length-sensing mechanism involved in neuronal symmetry breaking. Mol Syst Biol 6:394

Toriyama M, Shimada T, Kim KB, Mitsuba M, Nomura E, Katsuta K, Sakumura Y, Roepstorff P, Inagaki N (2006) Shootin1: A protein involved in the organization of an asymmetric signal for neuronal polarization. J Cell Biol 175:147-157

Troy TC, Arabzadeh A, Yerlikaya S, Turksen K (2007) Claudin immunolocalization in neonatal mouse epithelial tissues. Cell Tissue Res 330:381-388

Truffi M, Dubreuil V, Liang X, Vacaresse N, Nigon F, Han SP, Yap AS, Gomez GA, Sap J (2014) RPTPalpha controls epithelial adherens junctions, linking E-cadherin engagement to c-Src-mediated phosphorylation of cortactin. J Cell Sci 127:2420-2432

Wang YL (1985) Exchange of actin subunits at the leading edge of living fibroblasts: possible role of treadmilling. J Cell Biol 101:597-602

Weed SA, Parsons JT (2001) Cortactin: coupling membrane dynamics to cortical actin assembly. Oncogene 20:6418-6434

Wen YA, Liu D, Zhou QY, Huang SF, Luo P, Xiang Y, Sun S, Luo D, Dong YF, Zhang LP (2011) Biliary intervention aggravates cholestatic liver injury, and induces hepatic inflammation, proliferation and fibrogenesis in BDL mice. Exp Toxicol Pathol 63:277-284

Yadav N, Kanjirakkuzhiyil S, Kumar S, Jain M, Halder A, Saxena R, Mukhopadhyay A (2009) The therapeuic effect of bone marrow-drived liver cells in the phenotypic correction of murine hemophilia A. Blood 114:4552-4562

Yonemura S (2011) Cadherin-actin interactions at adherens junctions. Curr Opin Cell Biol 23:515-522

Figure Legends

Fig. 1 Identification and tissue distribution of shootin1b. (**a-a'**) Immunoblot analyses of E18.5 mouse brain lysate (10 μg proteins), purified recombinant shootin1a (5 ng) and purified recombinant shootin1b (5 ng) with anti-shootin1 antibody (**a**) and anti-shootin1b antibody (**a'**). Anti-shootin1 antibody reacts with shootin1a and shootin1b, while anti-shootin1b antibody recognizes specifically shootin1b. (**b**) Amino acid sequences of mouse, rat, and human shootin1b. Residues that are identical in all three sequences are boxed. (**c-c'**) Schematic representations of mouse shootin1a (**c**) and shootin1b (**c'**), showing three coiled-coil domains (CC1–3) and a single proline-rich region. Amino acid residues 454-631 are the shootin1b-specific region. (**d-d'**) Immunoblot analyses of shootin1b in adult mouse tissues (10 μg proteins) (**d**) and E18.5 mouse tissues (10 μg proteins) (**d'**) with anti-shootin1b antibody. Immunoblots with anti-actin antibody served as loading controls.

Fig. 2 Immunohistochemical localization of shootin1b in the mouse skin. Shootin1b immunoreactivity (green) and DAPI staining (red) in adult (**a-a'''**) and E18.5 (**b-b'''**) mouse skin. **a''**, **a'''**, **b''** and **b'''** are enlarged views of the areas 1, 2, 3 and 4, respectively. Shootin1b is located in all layers of the epidermis (Epi) and hair follicles (HF). BL, basal layer; CL, cornified layer; GL, granular layer; SG, sebaceous gland; SL, spinous layer. Arrowheads indicate shootin1b accumulation at cell-cell contact sites. Bars: (**a'** and **b'**) 30 μm; (**a''**, **a'''**, **b''** and **b'''**) 10 μm.

Fig. 3 Immunohistochemical localization of shootin1b in the mouse forestomach. Shootin1b immunoreactivity (green) and DAPI staining (red) in the adult (**a-a''**) and E18.5 (**b-b''**) mouse forestomach. **a''** and **b''** are enlarged views of the areas 1 and 2, respectively. KL, keratinized layer. Shootin1b is localized in the unkeratinized squamous epithelium. Arrowheads indicate shootin1b accumulation at cell-cell contact sites. Bars: (**a'** and **b'**) 30 μm; (**a''** and **b''**) 10 μm.

Fig. 4 Immunohistochemical localization of shootin1b in the mouse glandular stomach. (**a-a'''** and **b-b''**) Shootin1b immunoreactivity (green) and DAPI staining (red) in the adult (**a-a'''**) and E18.5 (**b-b''**) glandular stomach. Base, base zone; Neck, neck zone. (**c-c''''** and **d-d''**) Immunohistochemical colocalization of shootin1b (green) with a neck cell marker secretory protein TFF2 (red) (**c-c''''**) and a chief cell marker transcription factor Mist1 (red) (**d-d''**) in the adult glandular stomach. Blue indicates DAPI staining. **a''**, **a'''**, **b''** and **c'-c''''** are enlarged views of the areas 1, 2, 3 and 4, respectively. Arrows in **d''** indicate shootin1b expression in Mist1-positive mucous neck cells, while arrowheads in **a'''** and **b''** show shootin1b accumulation at cell-cell contact sites. Bars: (**a'**, **b'** and **c**) 30 μm; (**a''**, **a'''**, **b''** and **d''**) 10 μm; (**c''''**) 20 μm.

Fig. 5 Immunohistochemical localization of shootin1b in the mouse intestines. Shootin1b immunoreactivity (green) and DAPI staining (red) in the E18.5 mouse small intestine (**a-a”**), adult large intestine (**b-b”**) and E18.5 large intestine (**c-c”**). **a”**, **b”** and **c”** are enlarged views of the areas 1, 2 and 3, respectively. Arrowheads in a’’ indicate shootin1b accumulation at the lateral membrane. Bars: (**a’**, **b’** and **c’**) 30 μm; (**a’’**, **b’’** and **c’’**) 10 μm.

Fig. 6 Immunohistochemical localization of shootin1b in the mouse lung and liver. (**a-a”**, **b-b”** and **c-c”**) Shootin1b immunoreactivity (green) and DAPI staining (red) in the mouse adult lung (**a-a”**), E18.5 lung (**b-b”**) and adult liver (**c-c”**). **a”**, **b”**, and **c”** are enlarged views of the areas 1, 2 and 3, respectively. BD, bile duct; HC, hepatic cells; PV, portal vein; RE, respiratory epithelium. (**d-d”** and **e-e”**) Immunohistochemical colocalization of shootin1b (green) with a bile duct marker cytokeratin-19 (red) (**d-d”**) and a hepatic cell marker albumin (red) (**e-e”**) in the adult liver. Arrows in (**b”**) and (**c”**) indicate non-epithelial cells in the lung and cell-cell contact sites of hepatic cells, respectively. Arrowheads in (**c”**) indicate cell-cell contact sites of bile duct cells. Arrowheads in (**d”**) and (**e”**) indicate shootin1b expression in cytokeratin-19-positive bile duct cells and albumin-positive hepatic cells, respectively. Bars: (**a’**, **b’** and **c’**) 30 μm; (**a”**, **b”**, **c”** and **e”**) 10 μm; (**d”**) 5μm.

Fig. 7 Immunohistochemical localization of shootin1b in the mouse pancreas. (**a-a”** and **b-b”**) Shootin1b immunoreactivity (green) and DAPI staining (red) in the mouse adult pancreas (**a-a”**) and E18.5 pancreas (**b-b”**). **a”** and **b”** are enlarged views of the areas 1 and 2 respectively. PC, parenchymal cells of the pancreas; SD, secretory duct of the pancreas. (**c-c”**) Immunohistochemical colocalization of shootin1b (green) with an acinar cell marker amylase (red) in the adult pancreas. Arrowheads in (**c”**) indicate shootin1b expression in amylase-positive acinar cells. Bars: (**a’**and **b’**) 30 μm; (**a”**, **b”** and **c”**) 10 μm.

Fig. 8 Immunohistochemical localization of shootin1b in the mouse spleen. Shootin1b immunoreactivity (green), CD11c-immunoreactivity (red) and DAPI staining (blue) in the adult mouse spleen. **b-b”** and **c-c”** are enlarged views of the areas 1 and 2, respectively Arrows indicate co-localization of shootin1b with the dendritic cell marker CD11c. Bars: (**a’’**) 30 μm; (**b’’** and **c’’**) 10 μm.

Fig. 9 Shootin1b colocalizes with E-cadherin and cortactin in epithelial cells of the skin and glandular stomach. (**a-a’’’’** and **b-b’’’’**) Immunohistochemical colocalization of shootin1b (green) with E-cadherin (red) (**a-a’’’’**) and cortactin (red) (**b-b’’’’**) in E18.5 mouse skin. (**c-c’’’’** and **d-d’’’’**) Immunohistochemical colocalization of shootin1b (green) with E-cadherin (red) (**c-**

c””) and cortactin (red) (**d-d””**) in the E18.5 mouse glandular stomach. **a”’-a””’**, **b”’-b””’**, **c”’-c””’** and **d”’-d””’** are enlarged views of the indicated areas. Arrowheads indicate colocalization of shootin1b with E-cadherin and cortactin at cell-cell contact sites. Bars: (**a”**, **b”**, **c”** and **d”**) 30 μm; (**a””**, **b””**, **c””** and **d””**) 5 μm.

Fig. 10 Shootin1b colocalizes with E-cadherin and cortactin at cell-cell contact sites of cultured EpH4 cells. Immunocytochemical colocalization of shootin1b (green) with E-cadherin (**a-a”**) and cortactin (**b-b”**) in cultured EpH4 cells. The lower panels show vertical sections of the region indicated by the dotted lines. Arrowheads indicate colocalization of shootin1b with E-cadherin and cortactin at cell-cell contact sites. Bars: 20 μm.

Electronic Supplementary Material

Fig. S1 Two splice variants and isoforms of the mouse *shootin1* gene (**a**). The structure of the shootin1 locus and transcripts. (i) The structure of the mouse shootin1 genomic locus. (ii) Transcripts in the shootin1 locus. The shootin1 gene has two splice variants, a 3767-nt mRNA (NM_175172.4) encoding a protein of 456 amino acids and a 4081-nt mRNA (NM_001114312.1) encoding a protein of 631 amino acids. Gray and white boxes indicate exons and untranslated regions, respectively. Positions of stop codons (TAA and TGA) are shown. (**b**) Alignment of shootin1 isoforms. The amino acid sequences were obtained from the following sources: shootin1a (ABK56021.1) and shootin1b (NP_001107784.1).

Fig. S2 Immunoblot analyses of shootin1b in adult mouse tissues and E18.5 mouse tissues with anti-shootin1b antibody.

Whole scans of the immunoblotted membranes of Fig. 1d are shown.

Fig. S3 Control staining of the skin and forestomach without Anti-shootin1b Antibody. Two serial sections of the adult (**a**) and E18.5 (**b** and **e**) mouse skin, and the adult (**c**) and E18.5 (**d**) forestomach were immunostained: one section stained with anti-shootin1b antibody (shootin1b) and the other stained without the antibody (negative control). They were also co-stained with DAPI (**a-d**), anti-E-cadherin antibody (**e**) and anti-cortactin antibody (**e**) (red). CL, cornified layer; KL, keratinized layer. The data in (**e**) represent control data of those in Fig. 9. Bars: 50 μm.

Fig. S4. RT-PCR analysis of shootin1b mRNA in the skin.

RNA was extracted from the cornified layer and whole skin of P5 mouse. PCR was carried out by using shootin1b-specifc primers (left) and β-actin-specific primers (right) as a positive control. The PCR products were electrophoresed on a 2% agarose gel. The expected 233-bp shootin1b

and 165-bp β-actin PCR products were detected both in the cornified layer (lane 1) and whole skin (lane 2). M, 1 kb DNA ladder marker.

Further Reading

Ergin V, Erdogan M, Menevse A (2015) Regulation of shootin1 gene expression involves NGF-induced alternative splicing during neuronal differentiation of PC12 cells. Sci Rep 5:17931

After the submission of this paper, a report by Ergin et al. (2015) was published. This paper describes shootin1b expression in a PC12 cell line.

Fig. 1

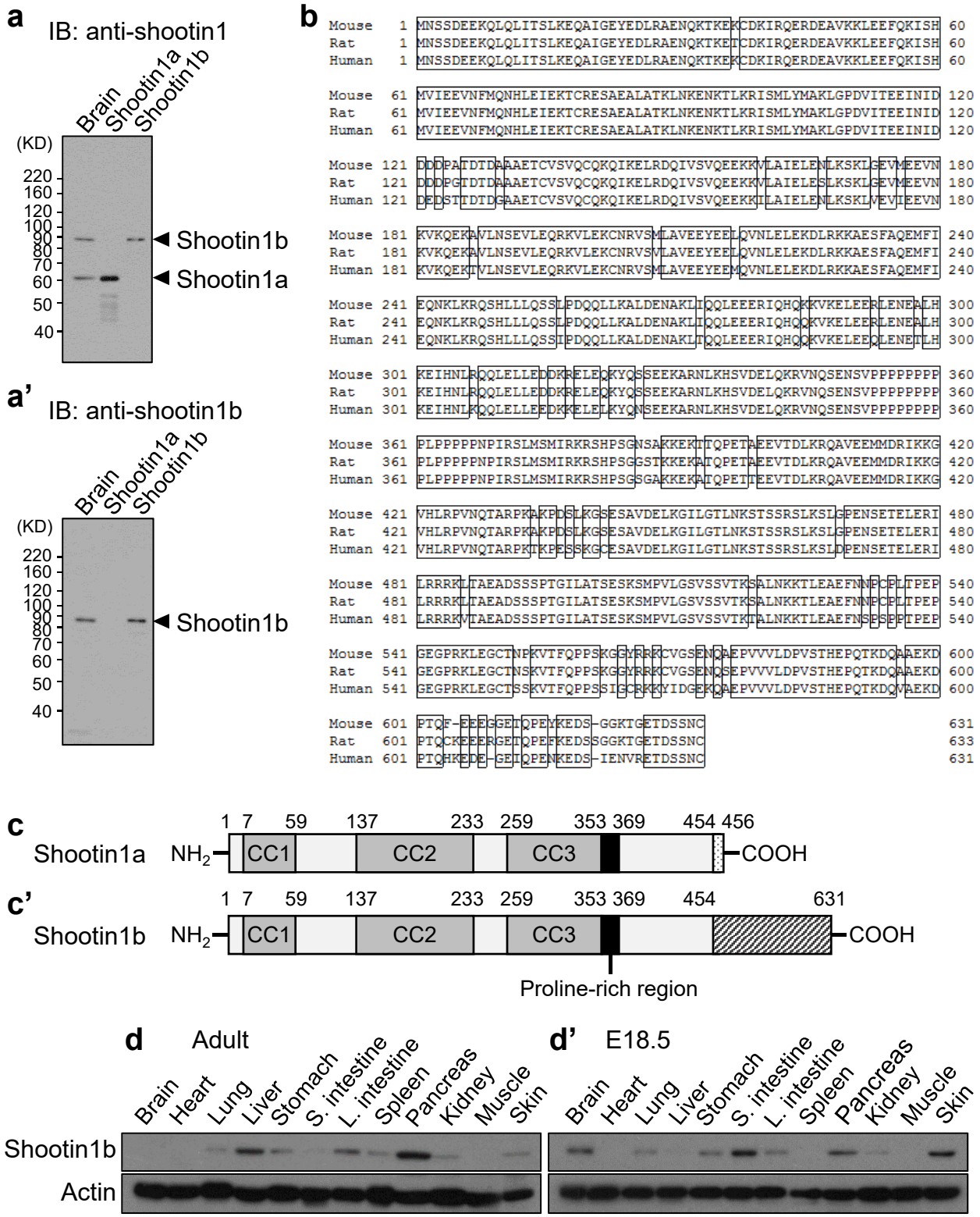
a
IB: anti-shootin1
Brain
Shootin1a
Shootin1b
(KD)
220
160
120
100
90
80
70
60
50
40
Shootin1b
Shootin1a
a'
IB: anti-shootin1b
Brain
Shootin1a
Shootin1b
(KD)
220
160
120
100
90
80
70
60
50
40
Shootin1b
b
Mouse 1 MNSSDEEKQLQLITSLKEQAIGEYEDLRAENQKTKEKCDKIRQERDEAVKKLEEFQKISH 60
Rat 1 MNSSDEEKQLQLITSLKEQAIGEYEDLRAENQKTKEICDKIRQERDEAVKKLEEFQKISH 60
Human 1 MNSSDEEKQLQLITSLKEQAIGEYEDLRAENQKTKEKCDKIRQERDEAVKKLEEFQKISH 60
Mouse 61 MVIEEVNFMQNHLEIEKTCRESAEALATKLNKENKTLKRISMLYMAKLGPDVITEEINID 120
Rat 61 MVIEEVNFMQNHLEIEKTCRESAEALATKLNKENKTLKRISMLYMAKLGPDVITEEINID 120
Human 61 MVIEEVNFMQNHLEIEKTCRESAEALATKLNKENKTLKRISMLYMAKLGPDVITEEINID 120
Mouse 121 DDDPATDTDAAAETCVSVQCQKQIKELRDQIVSVQEEKKVLAIELENLKSKLGEVMEEVN 180
Rat 121 DDDPGTDTDAAAETCVSVQCQKQIKELRDQIVSVQEEKKVLAIELESLKSKLGEVMEEVN 180
Human 121 DEDSTTDTDGAAETCVSVQCQKQIKELRDQIVSVQEEKKILAIELENLKSKLVEVIEEVN 180
Mouse 181 KVKQEKAVLNSEVLEQRKVLEKCNRVSMLAVEEYEELQVNLELEKDLRKKAESFAQEMFI 240
Rat 181 KVKQEKAVLNSEVLEQRKVLEKCNRVSVLAVEEYEELQVNLELEKDLRKKAESFAQEMFI 240
Human 181 KVKQEKTVLNSEVLEQRKVLEKCNRVSMLAVEEYEEMQVNLELEKDLRKKAESFAQEMFI 240
Mouse 241 EQNKLKRQSHLLLQSSLPDQQLLKALDENAKLIQQLEEERIQHQKKVKELEERLENEALH 300
Rat 241 EQNKLKRQSHLLLQSSLPDQQLLKALDENAKLIQQLEEERIQHQQKVKELEERLENEALH 300
Human 241 EQNKLKRQSHLLLQSSIPDQQLLKALDENAKLTQQLEEERIQHQQKVKELEEQLENETLH 300
Mouse 301 KEIHNLRQQLELLEDDKRELEQKYQSSEEKARNLKHSVDELQKRVNQSENSVPPPPPPPP 360
Rat 301 KEIHNLRQQLELLEDDKRELEQKYQSSEEKARNLKHSVDELQKRVNQSENSVPPPPPPPP 360
Human 301 KEIHNLKQQLELLEFDKKELELKYQNSEEKARNLKHSVDELQKRVNQSENSVPPPPPPPP 360
Mouse 361 PLPPPPPNPIRSLMSMIRKRSHPSGNSAKKEKTTQPETAEEVTDLKRQAVEEMMDRIKKG 420
Rat 361 PLPPPPPNPIRSLMSMIRKRSHPSGGSTKKEKATQPETAEEVTDLKRQAVEEMMDRIKKG 420
Human 361 PLPPPPPNPIRSLMSMIRKRSHPSGGAKKEKATQPETTEEVTDLKRQAVEEMMDRIKKG 420
Mouse 421 VHLRPVNQTARPKAKPDSLKGSESAVDELKGILGTLNKSTSSRSLKSLGPENSETELERI 480
Rat 421 VHLRPVNQTARPKAKPDSLKGSESAVDELKGILGTLNKSTSSRSLKSLGPENSETELERI 480
Human 421 VHLRPVNQTARPKTKPESSKGCESAVDELKGILGTLNKSTSSRSLKSLDPENSETELERI 480
Mouse 481 LRRRKLTAEADSSSPTGILATSESKSMPVLGSVSSVTKSALNKKTLEAEFNNPCPLTPEP 540
Rat 481 LRRRKLTAEADSSSPTGILATSESKSMPVLGSVSSVTKSALNKKTLEAEFNNPCPLTPEP 540
Human 481 LRRRKVTAEADSSSPTGILATSESKSMPVLGSVSSVTKTALNKKTLEAEFNSPSPPTPEP 540
Mouse 541 GEGPRKLEGCTNPKVTFQPPSKGGYRRKCVGSENQAEPVVVLDPVSTHEPQTKDQAAEKD 600
Rat 541 GEGPRKLEGCTNSKVTFQPPSKGGYRRKCVGSENQSEPVVVLDPVSTHEPQTKDQAAEKD 600
Human 541 GEGPRKLEGCTSSKVTFQPPSSIGCRKKYIDGEKQAEPVVVLDPVSTHEPQTKDQVAEKD 600
Mouse 601 PTQF-EEEGGEIQPEYKEDS-GGKTGETDSSNC 631
Rat 601 PTQCKEEERGEIQPEFKEDSSGGKTGETDSSNC 633
Human 601 PTQHKEDE-GEIQPENKEDS-IENVRETDSSNC 631
c
Shootin1a
NH2
1 7 59 137 233 259 353 369 454 456
CC1
CC2
CC3
COOH
c'
Shootin1b
NH2
1 7 59 137 233 259 353 369 454 631
CC1
CC2
CC3
COOH
Proline-rich region
d
Adult
Brain
Heart
Lung
Liver
Stomach
S. intestine
L. intestine
Spleen
Pancreas
Kidney
Muscle
Skin
Shootin1b
Actin
d'
E18.5
Brain
Heart
Lung
Liver
Stomach
S. intestine
L. intestine
Spleen
Pancreas
Kidney
Muscle
Skin

Fig. 2

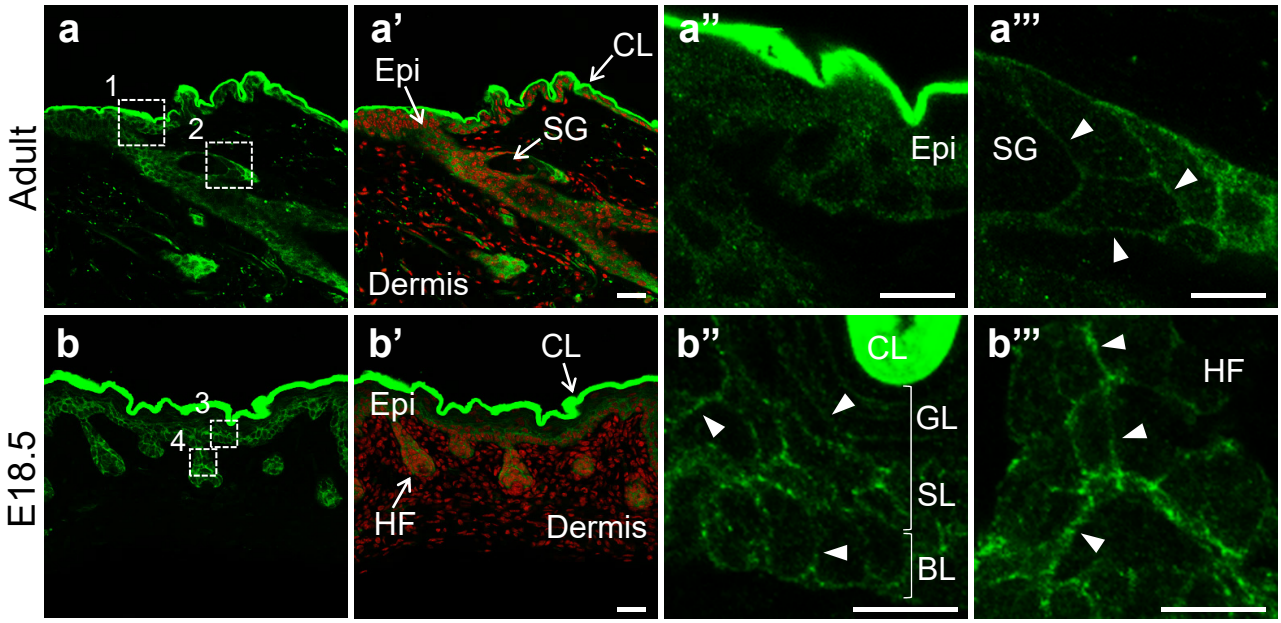

Fig. 3

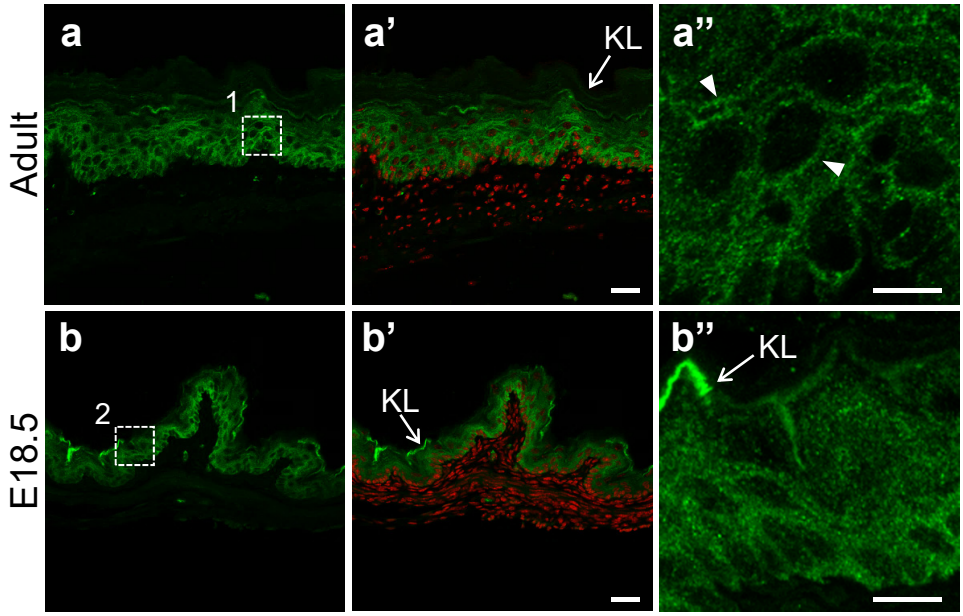

Fig. 4

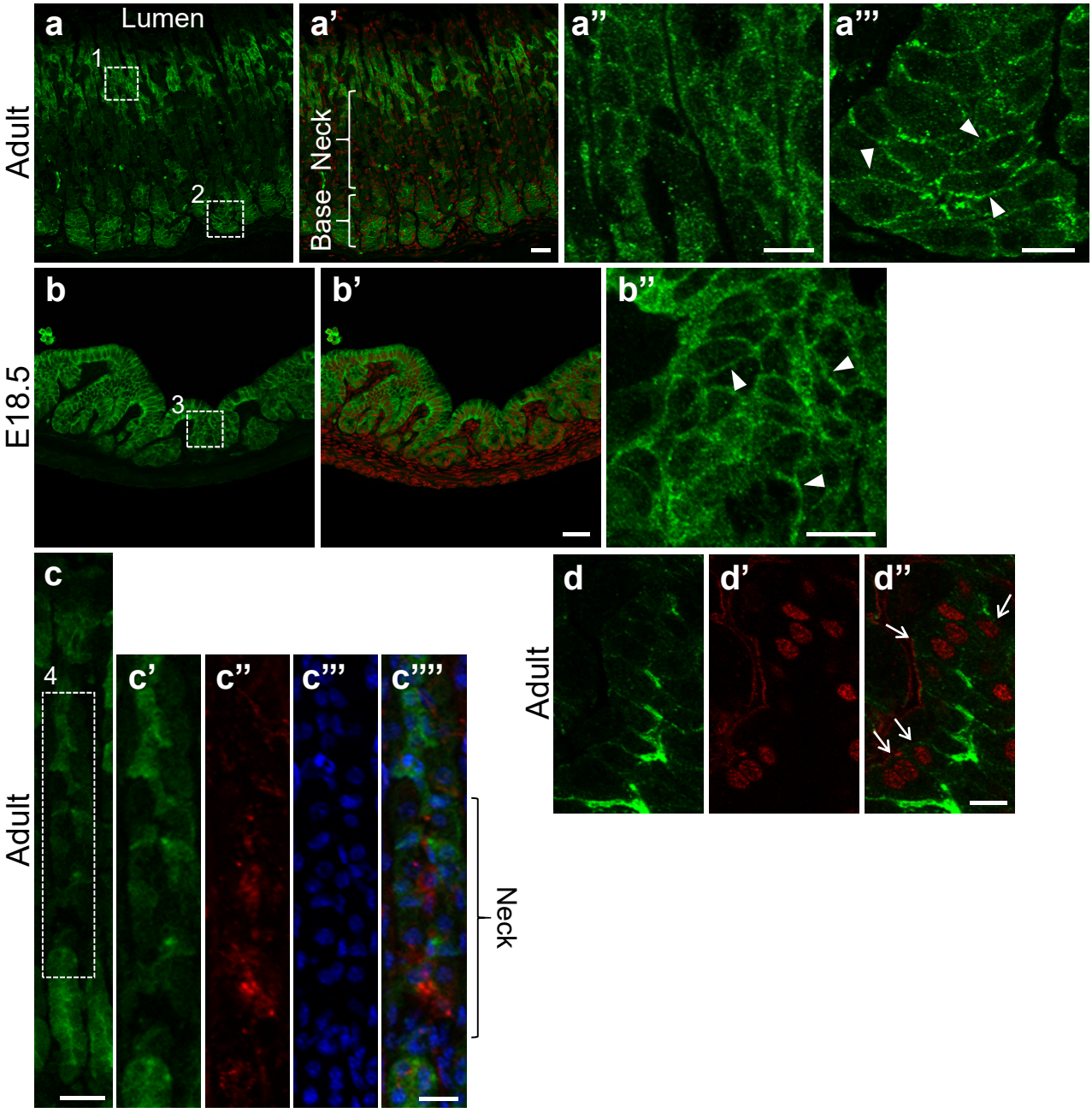
Adult
E18.5
Adult
Adult
a
Lumen
1
2
a'
Base
Neck
a''
a'''
b
3
b'
b''
c
4
c'
c''
c'''
c''''
Neck
d
d'
d''

Fig. 5

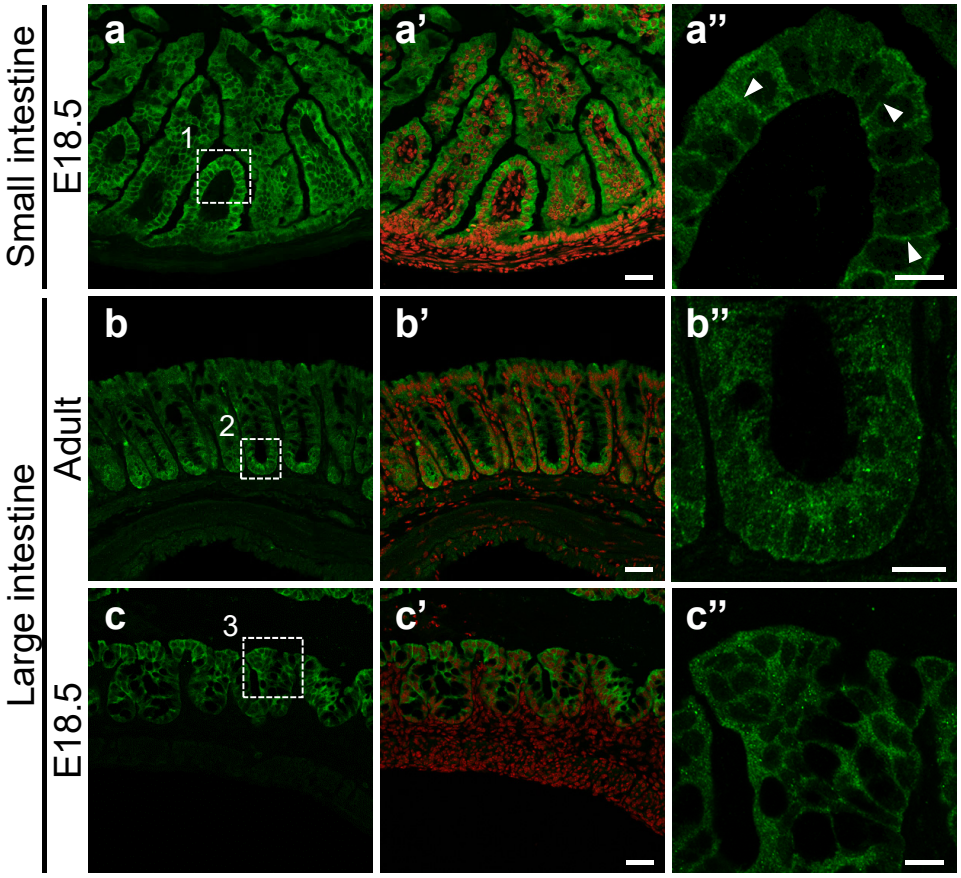
Small intestine
E18.5
Large intestine
Adult
E18.5
a
a'
a''
b
b'
b''
c
c'
c''
1
2
3

Fig. 6

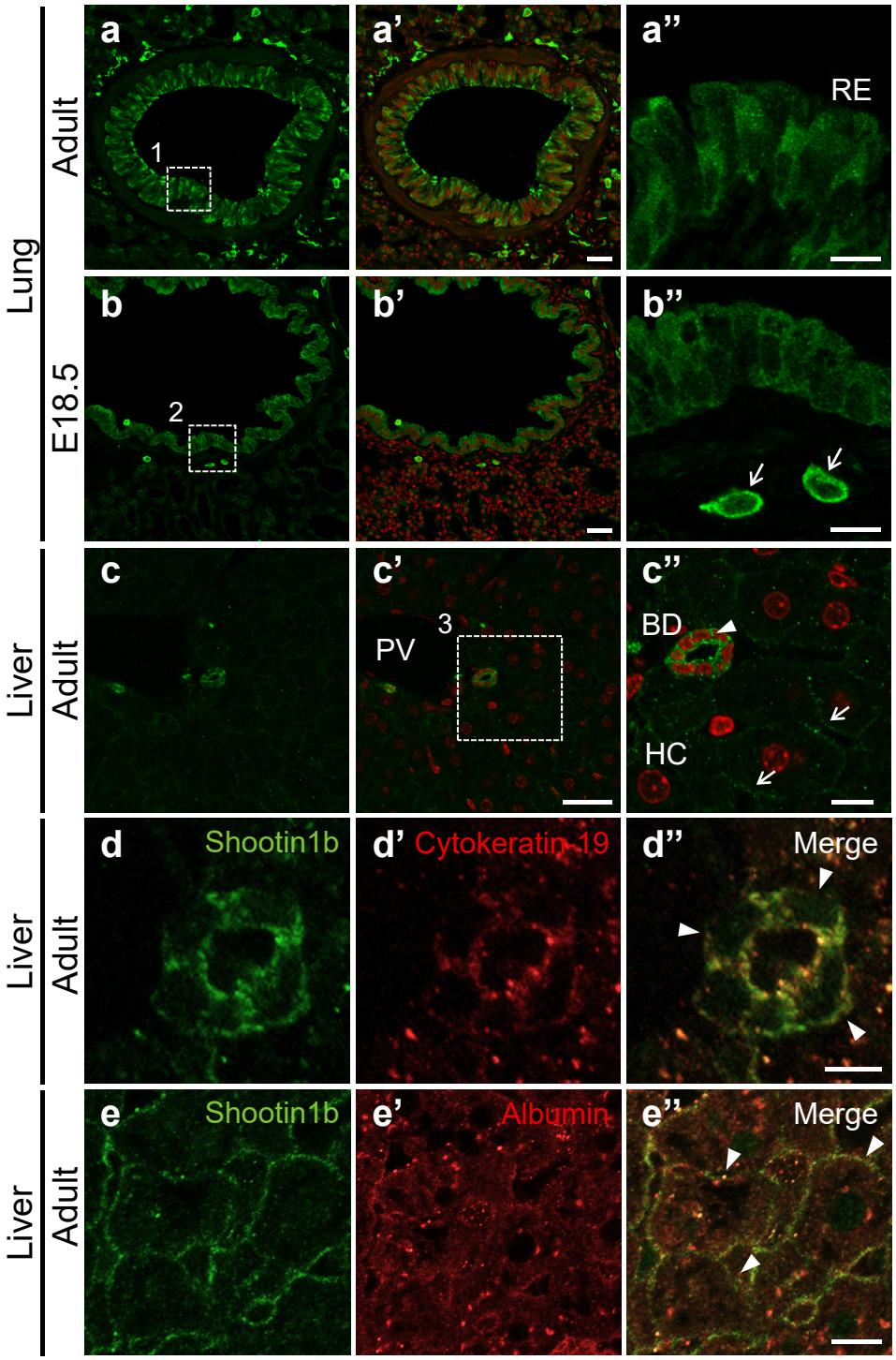
Lung
Adult
E18.5
Liver
Adult
Liver
Adult
Liver
Adult
a
a'
a''
RE
1
b
b'
b''
2
c
c'
c''
PV
3
BD
HC
d
Shootin1b
d' Cytokeratin-19
d''
Merge
e
Shootin1b
e'
Albumin
e''
Merge

Fig. 7

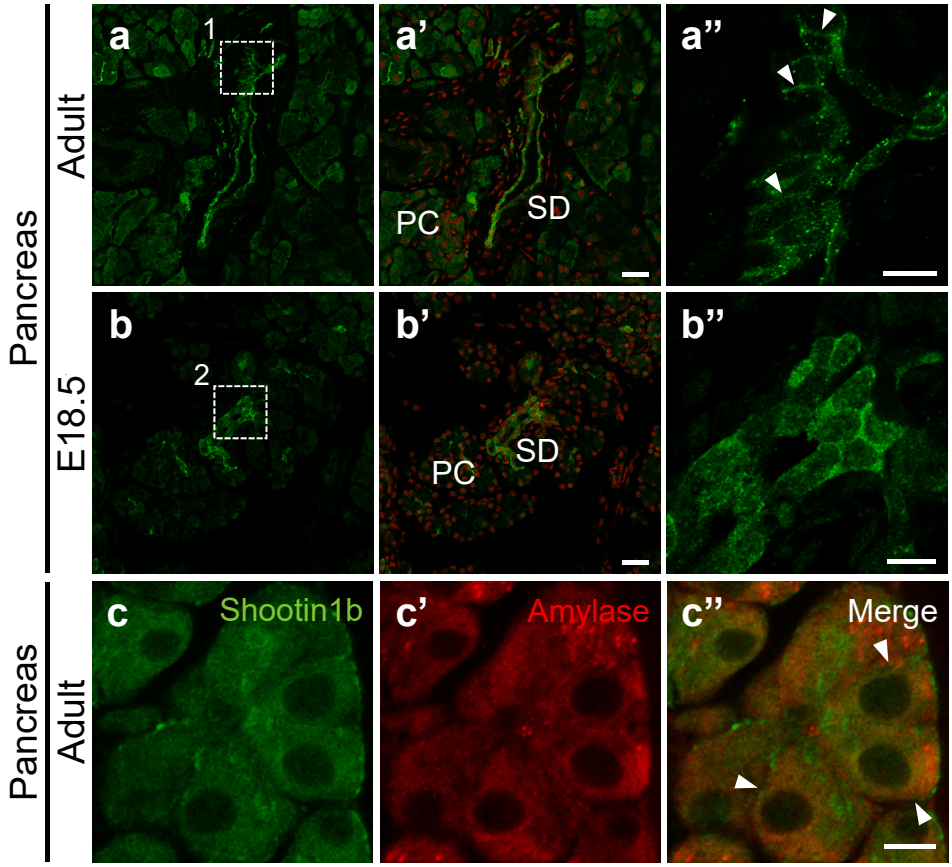
Pancreas
Adult
E18.5
Pancreas
Adult
a
1
a'
PC
SD
a"
b
2
b'
PC
SD
b"
c
Shootin1b
c'
Amylase
c"
Merge

Fig. 8

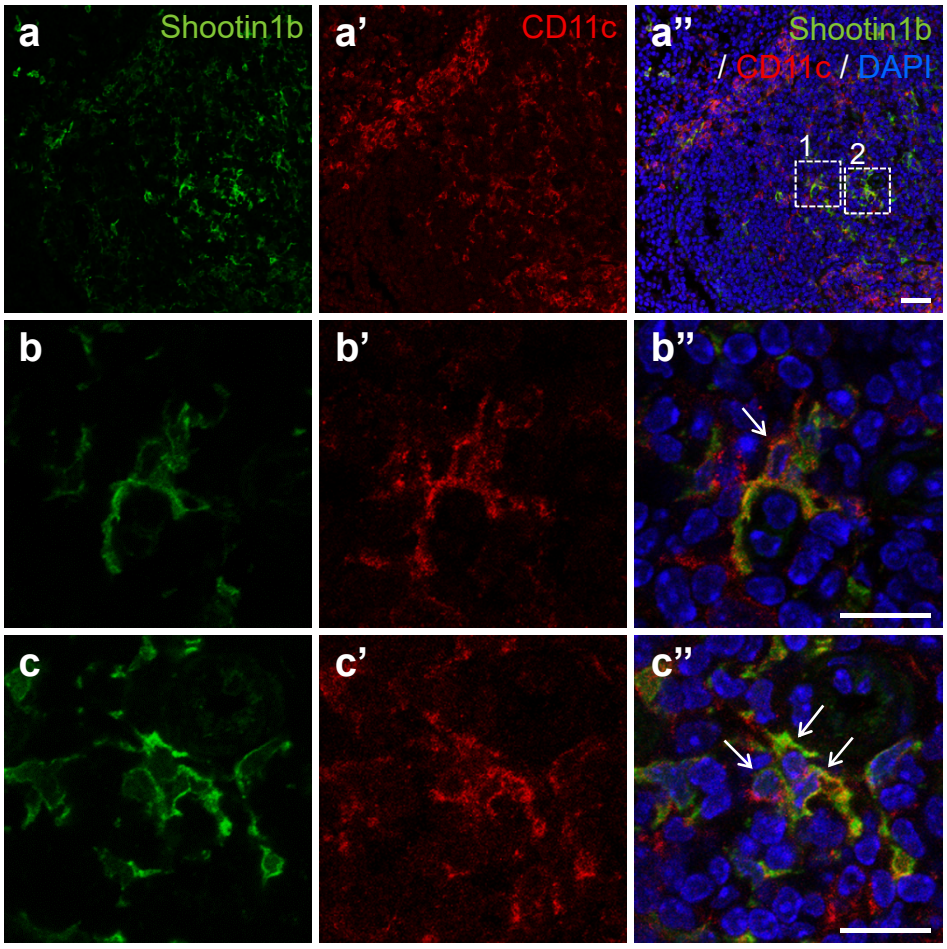

Fig. 9

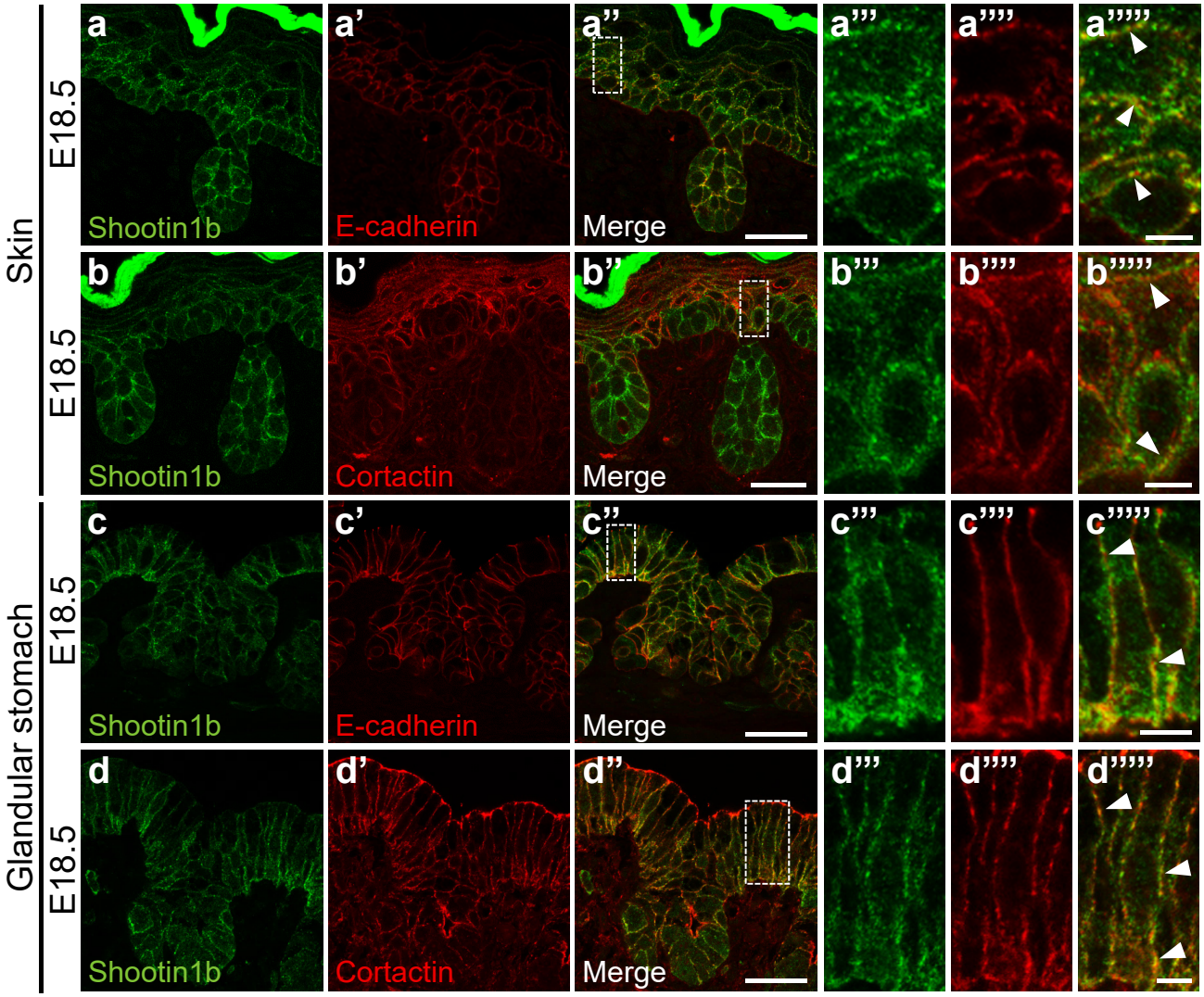
Skin
Glandular stomach
E18.5
E18.5
E18.5
E18.5
a
a'
a''
a'''
a''''
a'''''
b
b'
b''
b'''
b''''
b'''''
c
c'
c''
c'''
c''''
c'''''
d
d'
d''
d'''
d''''
d'''''
Shootin1b
E-cadherin
Merge
Shootin1b
Cortactin
Merge
Shootin1b
E-cadherin
Merge
Shootin1b
Cortactin
Merge

Fig. 10

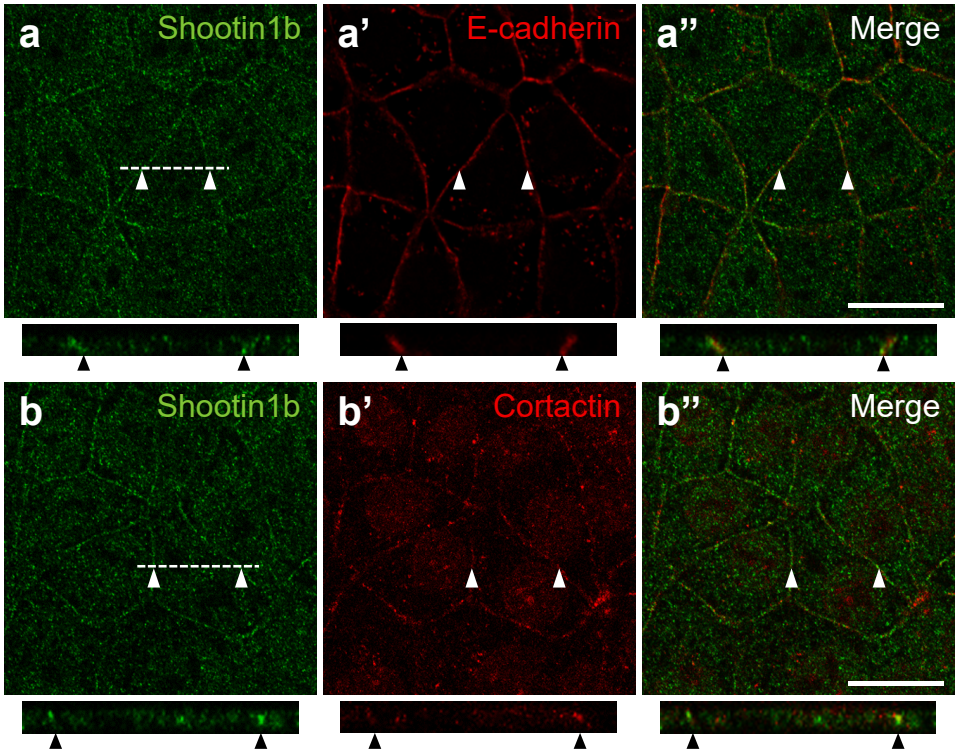
a
Shootin1b
a'
E-cadherin
a''
Merge
b
Shootin1b
b'
Cortactin
b''
Merge

Figure S1

a

(i)

shootin1

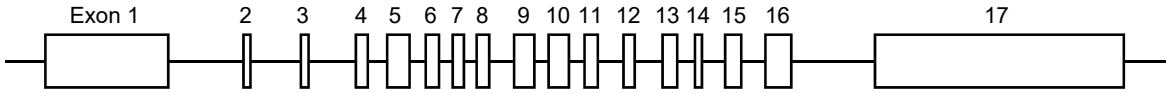

(ii)

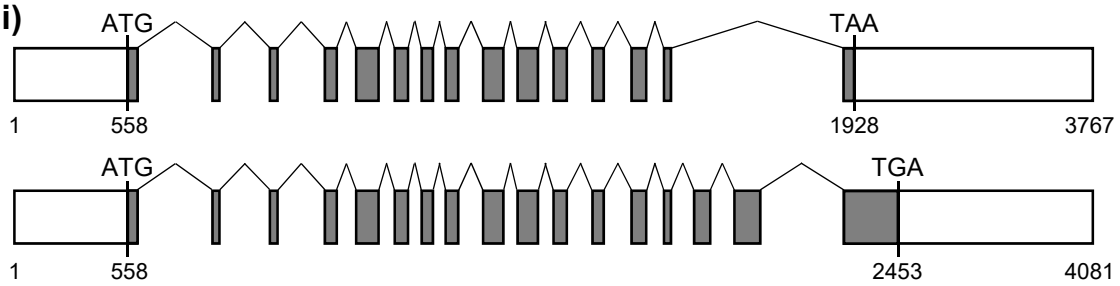

b

```
Shootin1a    1 MNSSDEEKQLQLITSLKEQAIGEYEDLRAENQKTKEKCDKIRQERDEAVKKLEEFQKISH 60
Shootin1b    1 MNSSDEEKQLQLITSLKEQAIGEYEDLRAENQKTKEKCDKIRQERDEAVKKLEEFQKISH 60

Shootin1a   61 MVIEEVNFMQNHLEIEKTCRESAEALATKLNKENKTLKRISMLYMAKLGPDVITEEINID 120
Shootin1b   61 MVIEEVNFMQNHLEIEKTCRESAEALATKLNKENKTLKRISMLYMAKLGPDVITEEINID 120

Shootin1a  121 DDDPATDTDAAAETCVSVQCQKQIKELRDQIVSVQEEKKVLAIELENLKSKLGEVMEEVN 180
Shootin1b  121 DDDPATDTDAAAETCVSVQCQKQIKELRDQIVSVQEEKKVLAIELENLKSKLGEVMEEVN 180

Shootin1a  181 KVKQEKAVLNSEVLEQRKVLEKCNRVSMLAVEEYEELQVNLELEKDLRKKAESFAQEMFI 240
Shootin1b  181 KVKQEKAVLNSEVLEQRKVLEKCNRVSMLAVEEYEELQVNLELEKDLRKKAESFAQEMFI 240

Shootin1a  241 EQNKLKRQSHLLLQSSLPDQQLLKALDENAKLIQQLEEERIQHQKKVKELEERLENEALH 300
Shootin1b  241 EQNKLKRQSHLLLQSSLPDQQLLKALDENAKLIQQLEEERIQHQKKVKELEERLENEALH 300

Shootin1a  301 KEIHNLRQQLELLEDDKRELEQKYQSSEEKARNLKHSVDELQKRVNQSENSVPPPPPPPP 360
Shootin1b  301 KEIHNLRQQLELLEDDKRELEQKYQSSEEKARNLKHSVDELQKRVNQSENSVPPPPPPPP 360

Shootin1a  361 PLPPPPPNPIRSLMSMIRKRSHPSGNSAKKEKTTQPETAEEVTDLKRQAVEEMMDRIKKG 420
Shootin1b  361 PLPPPPPNPIRSLMSMIRKRSHPSGNSAKKEKTTQPETAEEVTDLKRQAVEEMMDRIKKG 420

Shootin1a  421 VHLRPVNQTARPKAKPDSLKGSESAVDELKGILASQ---------------------- 456
Shootin1b  421 VHLRPVNQTARPKAKPDSLKGSESAVDELKGILGTLNKSTSSRSLKSLGPENSETELERI 480

Shootin1a  456 ------------------------------------------------------------ 456
Shootin1b  481 LRRRKLTAEADSSSPTGILATSESKSMPVLGSVSSVTKSALNKKTLEAEFNNPCPLTPEP 540

Shootin1a  456 ------------------------------------------------------------ 456
Shootin1b  541 GEGPRKLEGCTNPKVTFQPPSKGGYRRKCVGSENQAEPVVVLDPVSTHEPQTKDQAAEKD 600

Shootin1a  456 ------------------------------                               456
Shootin1b  601 PTQFEEEGGETQPEYKEDSGGKTGETDSSNC                               631
```

Figure S2

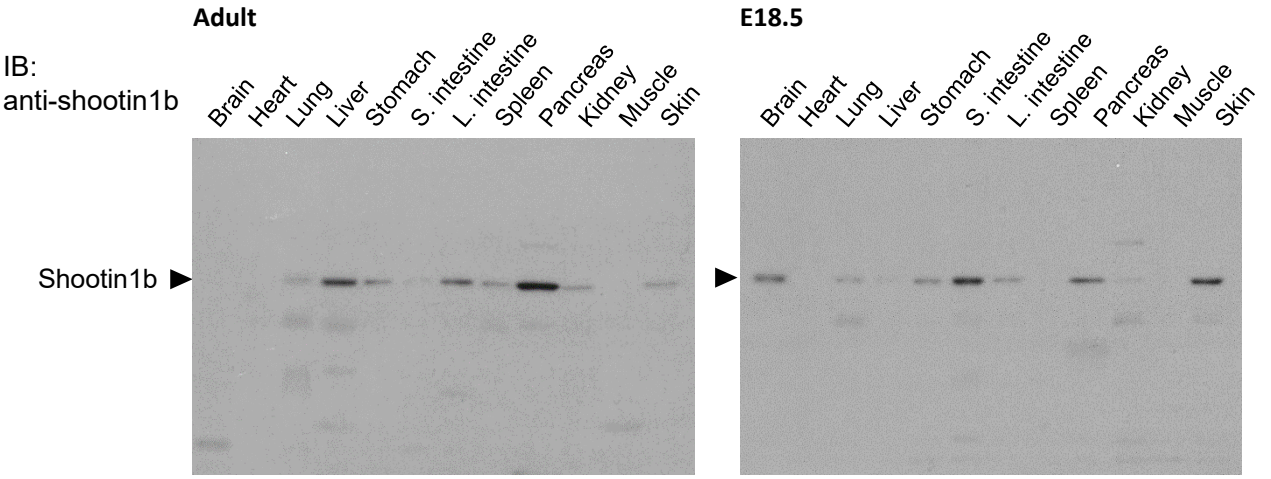
Adult
E18.5
IB:
anti-shootin1b
Brain
Heart
Lung
Liver
Stomach
S. intestine
L. intestine
Spleen
Pancreas
Kidney
Muscle
Skin
Shootin1b

Figure S3

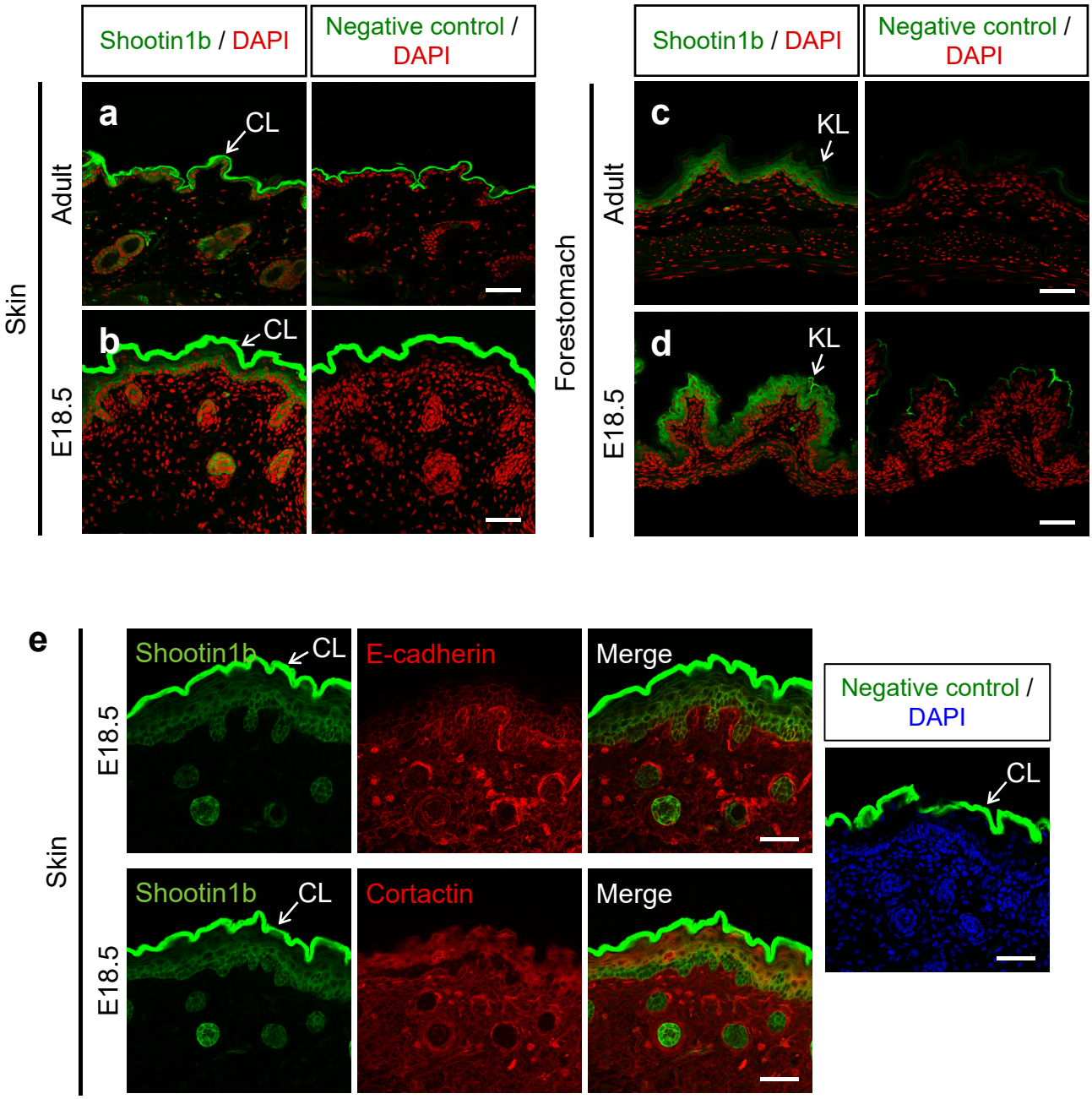
Shootin1b / DAPI
Negative control / DAPI
Skin
Adult
E18.5
a
CL
b
CL
Forestomach
Adult
E18.5
c
KL
d
KL
e
Shootin1b
CL
E-cadherin
Merge
Shootin1b
CL
Cortactin
Merge
Negative control / DAPI
CL

Figure S4